

Epitaxial $\text{Fe}_{3-x}\text{Ti}_x\text{O}_4$ films from magnetite to ulvöspinel by pulsed laser depositionT. C. Droubay,¹ C. I. Pearce,¹ E. S. Ilton,¹ M. H. Engelhard,¹ W. Jiang,¹ S. M. Heald,²
E. Arenholz,³ V. Shutthanandan,¹ and K. M. Rosso^{1,*}¹*Fundamental and Computational Sciences Directorate, Pacific Northwest National Laboratory, Richland, WA 99352, USA*²*Advanced Photon Source, Argonne National Laboratory, Argonne, IL 60439, USA*³*Advanced Light Source, Lawrence Berkeley National Laboratory, Berkeley, CA 94720, USA*

(Received 21 February 2011; revised manuscript received 11 August 2011; published 28 September 2011)

Epitaxial films along the $\text{Fe}_{3-x}\text{Ti}_x\text{O}_4$ (titanomagnetite) compositional series from pure end-members magnetite (Fe_3O_4) to ulvöspinel (Fe_2TiO_4) were successfully grown by pulsed laser deposition on $\text{MgO}(001)$ substrates. Characterization, including high-resolution x-ray diffraction, x-ray photoelectron spectroscopy, and synchrotron-based x-ray absorption and magnetic circular dichroism, consistently shows that Ti(IV) substitutes for Fe(III) in the inverse spinel lattice with a proportional increase in lattice Fe(II) concentration. No evidence of Ti interstitials, spinodal decomposition, or secondary phases was found in the bulk of the grown films. At the uppermost few nanometers of the Ti-bearing film surfaces, evidence suggests that Fe(II) is susceptible to facile oxidation and that an associated lower Fe/Ti ratio in this region is consistent with surface compositional alteration to a titanomaghemite-like composition and structure. The surfaces of these films nonetheless appear to remain highly ordered and commensurate with the underlying structure despite facile oxidation, a surface condition that is found to be reversible to some extent by heating in low-oxygen environments.

DOI: [10.1103/PhysRevB.84.125443](https://doi.org/10.1103/PhysRevB.84.125443)

PACS number(s): 73.22.-f

I. INTRODUCTION

Iron oxides as a group of materials have been studied extensively due to their potential technological use as well as their ubiquitous presence in soils. Among the iron oxides, ferrimagnetic spinel thin films have received considerable attention for prospective applications in microwave, magnetic storage, and spintronic devices.¹⁻³ Oxide spinel structure materials have the formula AB_2O_4 , in which tetrahedral (A) and octahedral (B) cations occupy some or all of the sites within a face-centered cubic close-packed lattice of oxygen anions. In the case of iron oxide inverse spinels (Fe_2MO_4 , $\text{M} = \text{Fe, Co, Ni, Mn, etc.}$), trivalent cations are split between the A and B sites, and divalent cations occupy only the B sites. The A- and B-site cation composition and distribution is critically important for the resulting electrical, magnetic, and redox properties of the material.

This paper deals with growth of epitaxial $\text{Fe}_{3-x}\text{Ti}_x\text{O}_4$ thin films, compositionally controlled along the binary solid-solution series from pure Fe_3O_4 magnetite ($x = 0.0$) to Fe_2TiO_4 ulvöspinel ($x = 1.0$). Intermediate compositions ($0.0 < x < 1.0$) are referred to as titanomagnetites. End-member magnetite is the archetypal ferrimagnet, in which high-spin iron cations are distributed [$\text{Fe}^{3+}_A(\text{Fe}^{2+}, \text{Fe}^{3+})_B\text{O}_4$] with opposing A- and B-site spin sublattices, imparting a net $4 \mu_B$ magnetization per formula unit. Systematic Ti substitution for Fe, nominally Ti(IV) for Fe(III), is attractive from the standpoint that it also proportionally increases lattice Fe(II) concentration for charge balance and reduces the net ferrimagnetic moment. However, the actual Ti/Fe cation site distribution and formal oxidation states remain somewhat controversial. Based on magnetization measurements, electrical transport, and thermoelectric data obtained from bulk solid solutions or bulk single crystals,^{4,5} several conflicting x -dependent cation distribution models have been presented.^{4,6-11} While these models are certainly relevant to the present study, inferences made from bulk materials are not

always applicable to systems with nanoscale dimensionality, such as thin films.^{12,13} It is thus of general scientific interest and potential technological value to examine and attain controlled thin film synthesis of this binary series.

There have been very few reported studies of epitaxial thin film growth along the magnetite-ulvöspinel series. Possible reasons include lack of readily available pure bulk end members for deposition precursor materials and challenges with spinodal decomposition at synthesis temperatures below the bulk consolute temperature ($\sim 490^\circ\text{C}$ for bulk phases).¹⁴ However, epitaxial Fe_3O_4 films have been successfully made for many years by a variety of deposition techniques, as reviewed by Chambers,¹⁵ including by pulsed laser deposition (PLD).^{13,16-19} In contrast to the substantial work on magnetite, to the best of our knowledge, only one group has reported titanomagnetite thin film synthesis. Murase *et al.* prepared and investigated solid-solution $0.4\text{Fe}_3\text{O}_4\cdot 0.6\text{Fe}_2\text{TiO}_4$ films using either $\text{MgO}(001)$ or $\alpha\text{-Al}_2\text{O}_3(0001)$ substrates.^{20,21}

In this paper, we report successful growth of epitaxial $\text{Fe}_{3-x}\text{Ti}_x\text{O}_4$ thin films from pure magnetite to ulvöspinel by PLD. $\text{MgO}(001)$ substrates were chosen because of prior success with magnetite and the relatively small lattice mismatch. The unit cell dimensions of Fe_3O_4 (8.396 Å) and Fe_2TiO_4 (8.544 Å) are nominally twice that of MgO (4.212 Å), resulting in lattice mismatches of only -0.33% and 1.4% , respectively. We present PLD synthesis growth conditions as well as detailed bulk and surface characterization of the thin films by reflection high-energy electron diffraction (RHEED), x-ray photoelectron spectroscopy (XPS), K - and L -edge x-ray absorption near-edge spectroscopy (XANES), high-resolution x-ray diffraction (HRXRD), x-ray absorption spectroscopy (XAS), and x-ray magnetic circular dichroism (XMCD).

II. EXPERIMENT

We developed PLD protocols for thin film growth targeted to the following five nominal compositions, $x = 0.00, 0.25,$

0.50, 0.75, and 1.00. Two main targets were used, depending upon the desired Ti concentration, an α -Fe₂O₃ target and an Fe₂TiO₄ target. The latter was a pressed and sintered ceramic PLD target. An additional pure TiO₂ target was also used for a few growth experiments to confirm the solid solubility and homogeneity of Ti in the magnetite lattice. All targets were 2-in diameter and commercially purchased from the Kurt J. Lesker Company. A KrF laser (248 nm) was used with a fluence of 2.4 J/cm² and a repetition rate of 2 Hz. The laser spot ($\sim 1 \times 10$ mm²) was rastered across a rotating target while the substrate was also rotating, allowing for uniform thickness across the substrate. Prior to growth, all targets were ablated for 15 min at a laser repetition rate of 10 Hz in 10 mTorr O₂ to eliminate carbonaceous surface contamination. Further laser-induced reduction of the Fe₂O₃ target was performed by ablating it at $< 1 \times 10^{-8}$ Torr O₂ for an additional 30 min prior to growth. A computer-controlled combination of laser pulses at the two different targets was calibrated and used when a stoichiometry other than that of the end members was desired. In a typical two-target growth procedure, each target was irradiated with a few laser pulses, followed by closing the shutter and moving the second target into the ablation position. The sequence would be repeated as many times as necessary to achieve the film thickness sought, typically ~ 50 – 100 nm. Intermediate composition Fe_{3-x}Ti_xO₄ films with Ti concentrations of $x = 0.25, 0.50,$ and 0.75 were routinely grown in this way.

Single-side epi-polished $10 \times 10 \times 1$ mm³ or $10 \times 10 \times 0.5$ mm³ MgO(001) substrates were used for all films. As-received MgO substrates were initially etched in H₃PO₄, rinsed in de-ionized water, and annealed under O₂ according to the procedure shown by Perry *et al.* to result in atomically flat, well-ordered, crystalline surfaces.^{22,23} Substrates were ultrasonically washed in isopropanol and methanol before introduction into the vacuum chamber. After sample introduction and prior to growth, the substrates were heated up to 500 °C in 10 mTorr O₂ to eliminate adventitious carbon from the growth surface. Oxygen flow into the chamber was stopped and the chamber pumped down prior to commencing PLD.

The oxygen partial pressure in the deposition chamber during film growth was $< 3 \times 10^{-9}$ Torr. The substrate temperature for all growths was ~ 350 °C, using a laser repetition rate of 2 Hz. Temperature, laser repetition rate, and oxygen partial pressure were chosen based on previous studies to eliminate Mg out-diffusion into the film during deposition from the underlying MgO substrate. For example, previous Fe₃O₄/MgO(001) deposition studies report significant film-substrate reaction and Mg out-diffusion at temperatures in excess of ~ 350 °C.^{24,25} Also, reports on the growth of Fe₃O₄ by PLD addressed the dependence of surface morphology and magnetic properties on pressure.¹⁸ Molten droplets and large particles ejected from the target during the laser ablation process are strongly forward directed along the laser plume axis. Elimination of the large particles was accomplished by growing in an N₂ atmosphere and by using an off-axis configuration, in which the substrate was ~ 7 cm away from the laser plume axis. No significant differences in structural quality or Ti incorporation were observed in films deposited in 1×10^{-7} Torr or 10 mTorr of N₂.

Some characterization methods required exposure to ambient atmosphere and were only pursued if the desired information pertained to the film bulk and was largely insensitive to possible surface oxidation. Air exposure time was consistently kept to the minimum required for sample transport into an ancillary characterization chamber or brief in-air analysis. Rutherford backscattering spectrometry (RBS) measurements were carried out using 2 MeV He⁺ ions. Backscattered helium ions were collected at the scattering angle of 150° using a surface barrier detector. The SIMNRA simulation program was used to model experimental RBS spectra, yielding the stoichiometries and thicknesses of the films.²⁶ In these simulations, the sample is divided into several thin layers of variable thickness and composition. This code utilizes the known Rutherford backscattering cross-section and all other experimental parameters, such as incident ion energy, atomic number of the ion, incident and scattering angles, energy calibration values for the detectors, solid angle of detection, and the total charge deposited by the incident beam together with the proposed structure, to calculate the theoretical spectrum. The composition profiles and film areal densities (in units of atoms/cm²) are then systematically varied until the best fit to experiment is obtained. The areal densities were then converted into actual film thickness (in nm) by using the bulk density of Fe₂O₃.

Epitaxial orientation, crystal quality, and lattice parameters of the films were determined in air using high-resolution x-ray diffraction (HRXRD) with a Philips X'Pert Materials Research Diffractometer (MRD) equipped with a fixed Cu anode operating at 45 kV and 40 mA. A hybrid monochromator, consisting of four-bounce double crystal Ge (220) and a Cu x-ray mirror, was placed in the incident beam path to generate monochromatic Cu K_α 1 x-rays ($\lambda = 1.54056$ Å) with a beam divergence of 12 arc seconds. The diffractometer exhibited an angular precision and reproducibility of 0.0001° and 0.0003°, respectively. XANES was performed in air on the PNC-CAT insertion device (20-ID) beamline at the Advanced Photon Source located at Argonne National Laboratory. The K-edge XANES is a sensitive probe of Fe and Ti oxidation states in the film bulk and provides qualitative information on their respective lattice locations. Sample rotation about the surface normal was used to minimize Bragg diffraction effects. Spectra collected with crossed (perpendicular and parallel) polarizations relative to the sample surface were appropriately averaged such that the XANES of the epitaxial films could be directly compared with those measured for metal foil(s) and oxide powder standards.

XPS of plasma-cleaned films that had been stored in an N₂ glove-box atmosphere was performed in a Gammatdata/Scienta SES 200 photoelectron spectrometer with a monochromatic Al-K_α (1486.7 eV) x-ray source. The angle between the x-ray beam and the axis of the analyzer is fixed at the magic angle of $\sim 54^\circ$, while the photoelectron emission angle can be varied between normal emission (bulk sensitive) and grazing emission (surface sensitive). RHEED was performed in a sample preparation chamber appended to the Scienta XPS system. Prior to RHEED analysis, adventitious carbon was cleaned from the sample surface using an electron cyclotron resonance oxygen plasma unit. The films were then reduced in vacuum by annealing to ~ 350 °C. *In-situ* heating experiments under vacuum ($\sim 5 \times 10^{-9}$ Torr) with a hydrogen partial pressure at 4.6×10^{-9} Torr in the XPS chamber were also

performed on the as-synthesized films at 100 and 350 °C in order to restore surface stoichiometry, using a Physical Electronics Quantum 2000 Scanning ESCA Microprobe. This Physical Electronics system uses a focused monochromatic Al-K α x-ray source and a spherical section electron energy analyzer. The instrument has a 16-element multichannel detection system. A 105 W x-ray beam focused to 100 μm diameter was rastered over a 1.4- \times 0.3-mm rectangle on the sample. The x-ray beam is incident normal to the sample, and the photoelectron detector is at 45° off normal, restricting the probing depth to the near surface ($\sim 3\lambda \cos \theta$), where λ is the inelastic mean free path of the electrons and θ is the emission angle measured from the surface normal. The high-energy resolution data was collected using a pass energy of 46.95 eV with a step size of 0.125 eV. For the Ag 3d_{5/2} line, these conditions produced a FWHM of 0.98 eV. Regional scans of the Fe 2p, O 1s, Ti 2p, and C 1s region were recorded, and the energy scale was referenced to adventitious C 1s at 285.0 eV. The Fe 2p were best fit by nonlinear least-squares using the CasaXPS curve resolution software, as described in the supplemental information section of Ilton *et al.*²⁷

Films were also heated at 300 °C on a hot plate for 10 min in an N₂ glove-box atmosphere to restore surface stoichiometry, and L_{2,3}-edge x-ray absorption and XMCD spectra were collected with circularly polarized light on beamline 4.0.2 at the Advanced Light Source (ALS) located at Lawrence Berkeley National Laboratory, using the eight-pole magnet end station.²⁸ The films were mounted on the copper sample manipulator with carbon tape and silver paint and loaded into the end station under anoxic conditions. Spectra were collected at 140 K. The XAS signal was monitored in total electron yield (TEY) mode, giving an effective probing depth of ~ 50 Å.²⁹ At each energy point, the XAS was measured for the two opposite magnetization directions by reversing the applied field of 0.6 T. The XAS spectra of the two magnetization directions were normalized to the incident beam intensity and subtracted from each other to obtain the XMCD spectrum.³⁰ For intermediate (titanomagnetite) compositions, XMCD spectra have four main peaks in the Fe L₃ edge with positive, negative, positive, and negative signals, which are related to the amounts of Fe *d*⁶ *Td* (~ 707 eV), *d*⁶ *Oh* (708 eV), *d*⁵ *Td* (~ 709 eV), and *d*⁵ *Oh* (~ 710 eV), respectively.³¹ End-member magnetite does not contain an Fe *d*⁶ *Td* component. To obtain the cation distribution over the three (magnetite) or four (titanomagnetite) Fe sites, measured XMCD spectra were fitted by means of a nonlinear least-squares analysis, using theoretical spectra previously calculated at the quantum mechanical level for each site. In these calculations, described in van der Laan and Kirkman³² and van der Laan and Thole,³³ 10 Dq crystal field parameters were taken as 1.2 and 0.6 eV for Fe *Oh* and *Td* sites. The results were convoluted by a Lorentzian of 0.3 (0.5) eV for the L₃ (L₂) edge to account for intrinsic core-hole lifetime broadening and by a Gaussian of 0.2 eV to account for instrumental broadening.

III. RESULTS & DISCUSSION

A. Film crystallinity and microstructure

Successful synthesis of phase-pure epitaxial $\text{Fe}_{3-x}\text{Ti}_x\text{O}_4$ films with high crystallinity and flat, well-ordered surfaces

depends on choice of substrate, laser repetition rate, temperature, and partial pressure of oxygen during deposition. The three most common substrates for the deposition of epitaxial Fe₃O₄ historically have been MgO, MgAl₂O₄, and α -Al₂O₃. Sapphire α -Al₂O₃(001) substrates were avoided because they tend to yield nanoscale phase separation at the interface.³⁴ MgO(001) was deemed the most suitable substrate to minimize any interfacial strain-induced effects because of its small lattice mismatch with Fe₃O₄(001), as documented by Parames *et al.*³⁵ With respect to oxygen partial pressure, it was found that Fe_{3-x}Ti_xO₄ grew best at $< 3 \times 10^{-9}$ Torr. Films with a range of thicknesses from 10 to 100 nm were synthesized. Unless otherwise stated, data shown are from samples of thickness ~ 100 nm. Shown in Fig. 1(a) are the typical RHEED patterns obtained for the initial MgO(001) substrate, a ~ 10 -nm Fe₂TiO₄/MgO(001) film, and the same film after annealing to ~ 300 °C following 30 min in an electron cyclotron resonance oxygen plasma to clean off adventitious carbon. As seen in the streaky RHEED pattern from the annealed film following plasma cleaning, the surface is exceptionally flat and well ordered. Only pure Fe₃O₄ exhibits quarter-order streaks (not shown) along [100] relative to MgO, consistent with the reported ($\sqrt{2} \times \sqrt{2}$) R45° Fe₃O₄(001) surface reconstruction [Fig. 1(b)].^{36,37} With the addition of Ti, neither the Fe_{2.75}Ti_{0.25}O₄, Fe_{2.5}Ti_{0.5}O₄, Fe_{2.25}Ti_{0.75}O₄ films nor Fe₂TiO₄(001) were found to exhibit this reconstruction,

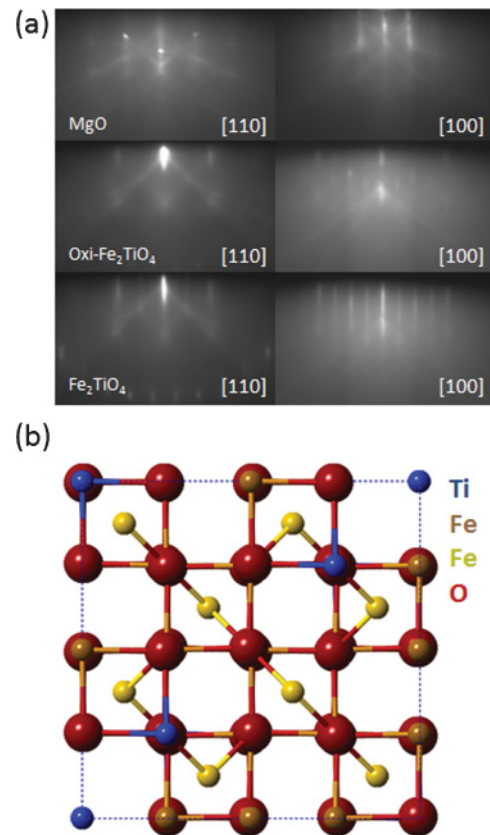


FIG. 1. (Color online) Typical RHEED patterns obtained from (top) an MgO(001) substrate and (middle) an epitaxially-grown Fe₂TiO₄(001) film which has been exposed to oxygen and (bottom) vacuum-annealed at 300 °C; and a ball-and-stick model of the nominal (001) bulk truncation of Fe₂TiO₄

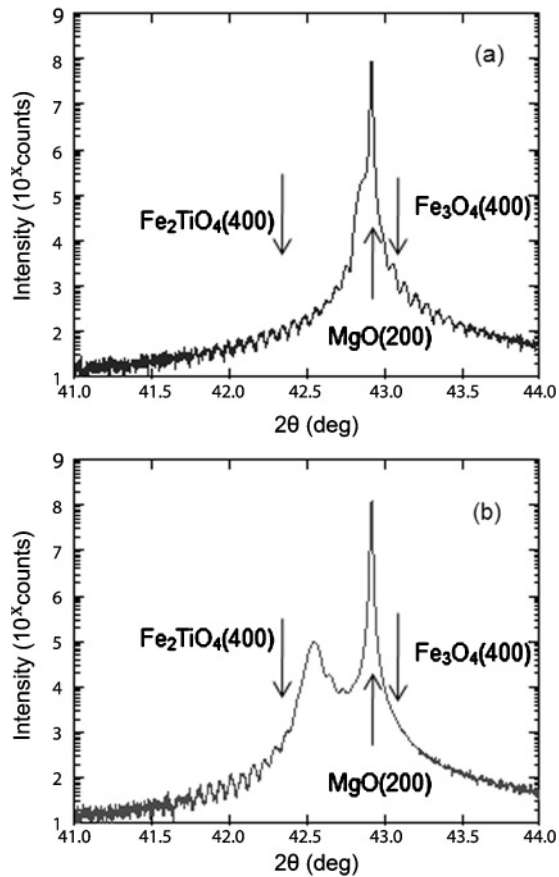


FIG. 2. (a) HRXRD of the $\text{Fe}_{2.75}\text{Ti}_{0.25}\text{O}_4/\text{MgO}(001)$ film and (b) the $\text{Fe}_{2.25}\text{Ti}_{0.75}\text{O}_4/\text{MgO}(001)$ film grown by pulsed laser deposition showing the shift in Bragg peak with Ti concentration.

suggesting perhaps a bulk (polar) termination (e.g. Pentcheva *et al.*³⁸). Curiously, upon exposure to significant oxygen or ambient atmosphere, the surface appears to roughen, as seen in the modulation along the RHEED streaks, but does not appear to undergo a phase transition, as seen for pure Fe_3O_4 upon exposure to water vapor.³⁹

The Fe:Ti ratio in the films was confirmed by RBS analysis of the nominally $x = 0.25$ and 0.50 films with the compositions quantitatively determined to be $\text{Fe}_{2.74}\text{Ti}_{0.26}\text{O}_4$ and $\text{Fe}_{2.48}\text{Ti}_{0.52}\text{O}_4$, respectively. The structural quality of the films is confirmed with HRXRD, as illustrated for $\text{Fe}_{2.5}\text{Ti}_{0.25}\text{O}_4$ [Fig. 2(a)] and $\text{Fe}_{2.25}\text{Ti}_{0.75}\text{O}_4$ [Fig. 2(b)], which reveal (001)-oriented films with high crystallinity. Two distinct Bragg peaks are visible at $2\theta = 42.5^\circ$ and 42.8° for the higher Ti concentration [Fig. 2(b)], corresponding to the titanomagnetite film and MgO, respectively. As can be seen by comparison of Figs. 2(a) and 2(b), the Bragg peak associated with the film shifts to a lower angle as the Ti concentration increases. This decrease in the Bragg angle corresponds to an increasing unit cell dimension with increasing Ti content, consistent with expectations from related studies of the bulk phases.³¹ A strain-induced tetragonal distortion is expected for growth on MgO(001) because of the small but finite lattice mismatch.¹⁵ The out-of-plane lattice parameters measured by HRXRD increase from 8.434 to 8.492 Å as x increases from 0.25 to 0.75 , which is very similar to the increase seen in the

corresponding bulk phases.³¹ From the combined RHEED and HRXRD data, it can be concluded that the $\text{Fe}_{3-x}\text{Ti}_x\text{O}_4$ films grow epitaxially on the MgO substrate with the desired inverse spinel crystal structure and (001) surface orientation. In addition, we can infer from the monotonic change in lattice constant with titanium concentration that the majority of Ti atoms are substituting for Fe in the cationic sublattice. Within the sensitivity of HRXRD, there is no indication of either secondary phases or spinodal decomposition to distinct Fe_3O_4 and Fe_2TiO_4 phases within any of the $\text{Fe}_{3-x}\text{Ti}_x\text{O}_4$ films.

B. Bulk film cation charge state and local structure

While phase separation to domains larger than ~ 5 – 10 nm would have been detected by HRXRD, finer-scale separation could have been overlooked. Fe and Ti K -edge XANES with fluorescence detection was therefore used as a more sensitive probe of the atomic structure. Because this technique is able to probe the entire film in addition to being element specific, it provides information on Ti and Fe oxidation states as well as the local structure around these cations in the bulk of the film. Samples with ~ 10 nm thickness were used to better accentuate the signal from the oxidized surface layer.

Figure 3(a) shows Ti K -edge XANES for three different $\text{Fe}_{3-x}\text{Ti}_x\text{O}_4/\text{MgO}(001)$ films. By comparing the inflection point of the Ti absorption spectra with those from Ti standards, it is clear that Ti is in the +4 formal charge state for all Ti concentrations up to and including Fe_2TiO_4 . Specific comparison is made between Fe_2TiO_4 and TiO_2 powder in Fig. 3(b). Furthermore, because of differences in the overall line shape, the majority of Ti in the films is not from a secondary phase, such as TiO_2 , although the presence of small amounts of this phase at the surface cannot be ruled out. This is also true of a separate $\text{Fe}_2\text{TiO}_4/\text{MgO}(001)$ film grown by PLD using Fe_2O_3 and TiO_2 targets, establishing that small amounts of phase separation nominally expected in a typical pressed and sintered ceramic target (e.g. the commercial Fe_2TiO_4 PLD target) does not lead to detectable phase separation in the resulting film.

Figure 3(c) shows Fe K -edge XANES from the same three films as in Fig. 3(a) with Fig. 3(d) showing the powder XANES spectra from multiple standard iron oxides. Comparison of the inflection point in the Fe absorption edges recorded for the titanomagnetite films with those from the standards provides a basis to determine an average formal oxidation state for the iron component using FeO for the Fe(II) standard and α - Fe_2O_3 as the Fe(III) standard. In addition, although the Fe XANES spectra from the Fe_2TiO_4 films are offset on the y axis, for clarity, the curves are displaced slightly in energy from each other, indicating that the Fe(II)/Fe(III) ratio systematically increases with increasing Ti concentration as expected.

Comparing the Ti and Fe x-ray absorption line shapes from the films, it is clear that the relatively small pre-edge feature is stronger for the Ti K edge than for the Fe K edge. The pre-edge feature is due to a $1s$ -to- $3d$ transition, which is formally dipole forbidden but increases in intensity through local mixing between the $3d$ and $4p$ states in tetrahedral symmetry.^{40,41} In a study of Ti-based catalysts, Thomas and Sankar⁴² showed the dependence of the Ti K -pre-edge peak

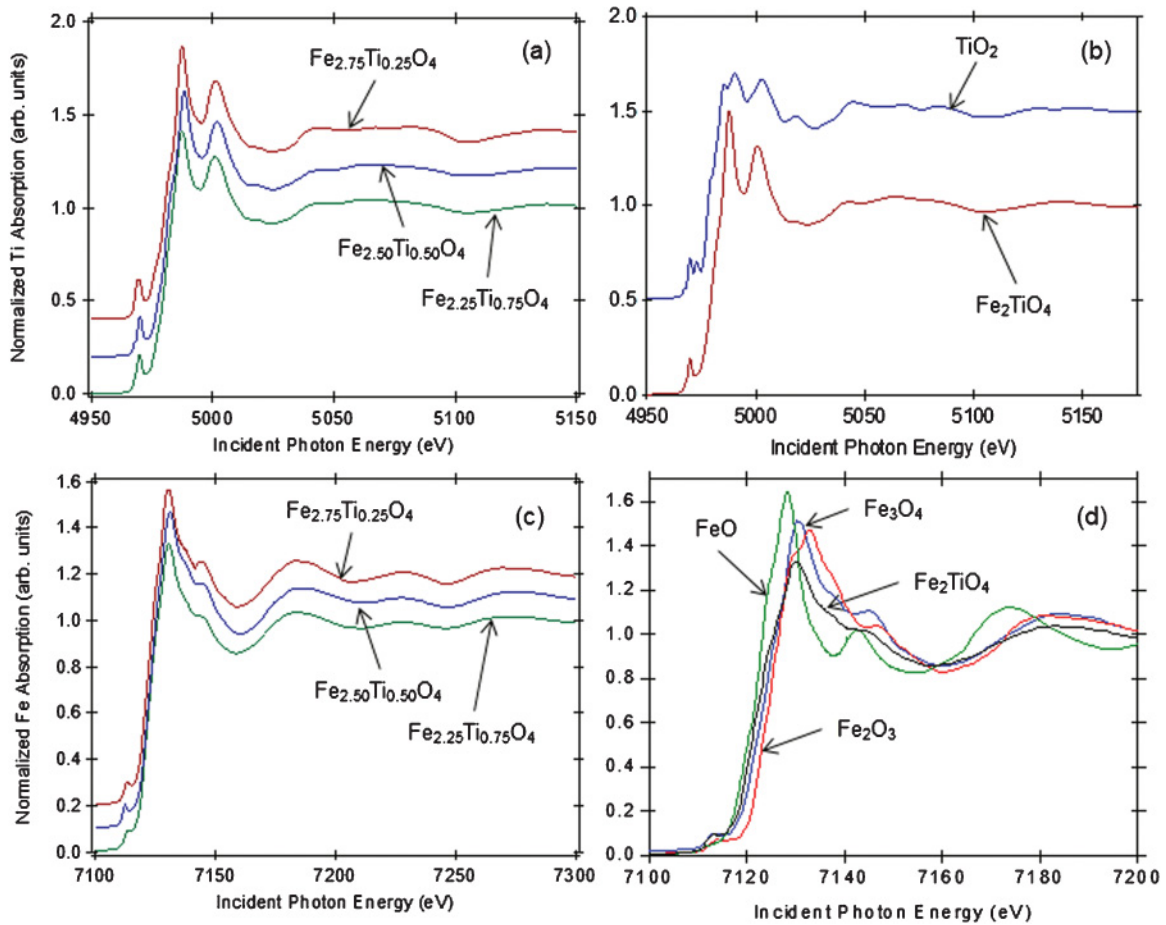


FIG. 3. (Color online) (a) Ti K -edge XANES spectra for films: $\text{Fe}_{2.75}\text{Ti}_{0.25}\text{O}_4/\text{MgO}(001)$, $\text{Fe}_{2.50}\text{Ti}_{0.50}\text{O}_4/\text{MgO}(001)$, and $\text{Fe}_{2.25}\text{Ti}_{0.75}\text{O}_4/\text{MgO}(001)$. (b) Comparison of the Ti K -edge XANES of Fe_2TiO_4 and TiO_2 showing that Ti is present as Ti(IV) in Fe_2TiO_4 . (c) Fe K -edge XANES spectra for films: $\text{Fe}_{2.75}\text{Ti}_{0.25}\text{O}_4/\text{MgO}(001)$, $\text{Fe}_{2.50}\text{Ti}_{0.50}\text{O}_4/\text{MgO}(001)$, $\text{Fe}_{2.25}\text{Ti}_{0.75}\text{O}_4/\text{MgO}(001)$. (d) Comparison of the Fe K -edge XANES for the $\text{Fe}_2\text{TiO}_4/\text{MgO}(001)$ film with Fe-oxide standards (FeO , Fe_3O_4 , and Fe_2O_3).

intensity on the coordination of the oxygen atoms around the central Ti(IV). However, since the intensity of the pre-edge peak does not increase with Ti concentration, it seems unlikely that this is a result of the sequential substitution of Ti cations into A sites in the $\text{Fe}_{3-x}\text{Ti}_x\text{O}_4$ film. Alternatively, it is possible that, although Ti(IV) has substituted into the B-site, there may be a next-nearest neighboring cation vacancy that promotes tetragonal strain and thus increases the pre-edge peak intensity. Cationic vacancy or interstitial cation concentrations, which are dependent upon oxygen fugacity, have been suggested by Morris *et al.*⁴³ as a means to reconcile data on the electronic structure of Nb-doped TiO_2 . Furthermore, cation vacancies were concluded to be the predominant defects at high-oxygen activities by Aggarwal and Dieckmann in titanomagnetites.⁴⁴ It thus appears plausible that a small population of Ti-associated B-site Fe vacancies may explain the presence of the Ti K -pre-edge feature. As discussed further below, such vacancies would break the requirement that the Fe(II) concentration increase concomitantly with Ti(IV) substitution to preserve charge neutrality for that population of sites.

The conclusion that Ti(IV) is predominantly substituting in the cation sublattice is corroborated by comparing the XANES

line shapes for Fe in the bulk Fe_3O_4 standard, Fe in the Fe_2TiO_4 film, and Ti in the Fe_2TiO_4 film, as seen in Fig. 4(a). The energy scales have been shifted to align inflection points and facilitate this comparison. Here, the Fe_3O_4 line shape can be well approximated by a linear combination of Ti and Fe film spectra, consistent with Ti(IV) replacement of the Fe(III) component in Fe_3O_4 . This provides further confirmation that the films are nearly free of secondary phases and spinodal decomposition within detection limits of the applied techniques.

To quantitatively determine the average Fe oxidation state within the films, a plot of the measured inflection point as a function of x is shown in Fig. 4(b). The average Fe oxidation state for all of the films can be seen to lie directly along the line defined by FeO and $\alpha\text{-Fe}_2\text{O}_3$. However, this analysis also suggests that the average Fe oxidation state is slightly higher than expected based on stoichiometry. For example, the average Fe oxidation state in the Fe_2TiO_4 thin film is estimated to be ~ 2.2 , whereas it should be 2.0 in a perfectly stoichiometric film. This discrepancy further confirms the possible presence of cation vacancies induced by oxidation at Fe sites in the near-surface region. In order to explore this possibility, we performed a range of surface-sensitive spectroscopic analyses as described below.

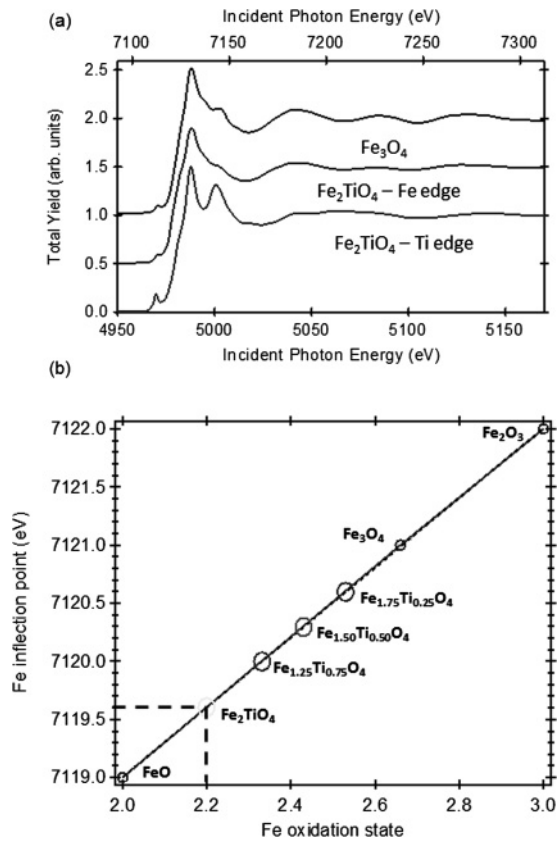


FIG. 4. (a) Fe *K*-edge XANES from Fe₃O₄ as well as Fe and Ti *K*-edge XANES from Fe₂TiO₄, indicating that Ti substitutes for Fe in the cationic sublattice. (b) Comparison of the inflection points for several (large circles) Fe_{3-x}Ti_xO₄/MgO(001) films along with those determined for (small circles) FeO, Fe₃O₄, and Fe₂O₃ standards that shows the linear trend of Fe(III)/Fe(II) ratio with Ti concentration parameter *x*.

C. Film surface properties

One possible near-surface composition and structure consistent with the bulk-dominated film measurements is one in which the upper few nanometers are oxidized to Ti(IV)-doped Fe_{8/3}O₄ maghemite (titanomaghemite). Maghemite is the inverse spinel solid-solution end member of Fe₃O₄ oxidation, and an analogous topotactic binary exists between titanomagnetite-titanomaghemite. As shown by O'Reilly,⁴⁵ the mechanism of maghematization in titanomagnetites involves oxidation of structural Fe(II) with concomitant removal of Fe(III) from the octahedral sublattice in a 3:1 ratio. This process increases the Fe(III)/Fe(II) ratio and reduces the Fe/Ti ratio. Such a surface layer would provide for the observations above of a higher-than-expected Fe(III) concentration in the films, a surface unit cell of identical symmetry and approximately equivalent dimensions to the underlying film bulk, and an intrinsic B-site vacancy component consistent with interpretation of the Ti *K*-pre-edge peak intensity. This altered surface layer may act to either passivate the surface or at least slow the oxidation of more reduced films, such as Fe₂TiO₄, as seen by some researchers.⁴⁶ To investigate the surface layer in more detail and the potential for surface re-equilibration, the Fe₃O₄ and Fe₂TiO₄ end-member films were examined with XPS and Fe *L*_{2,3}-edge XAS/XMCD

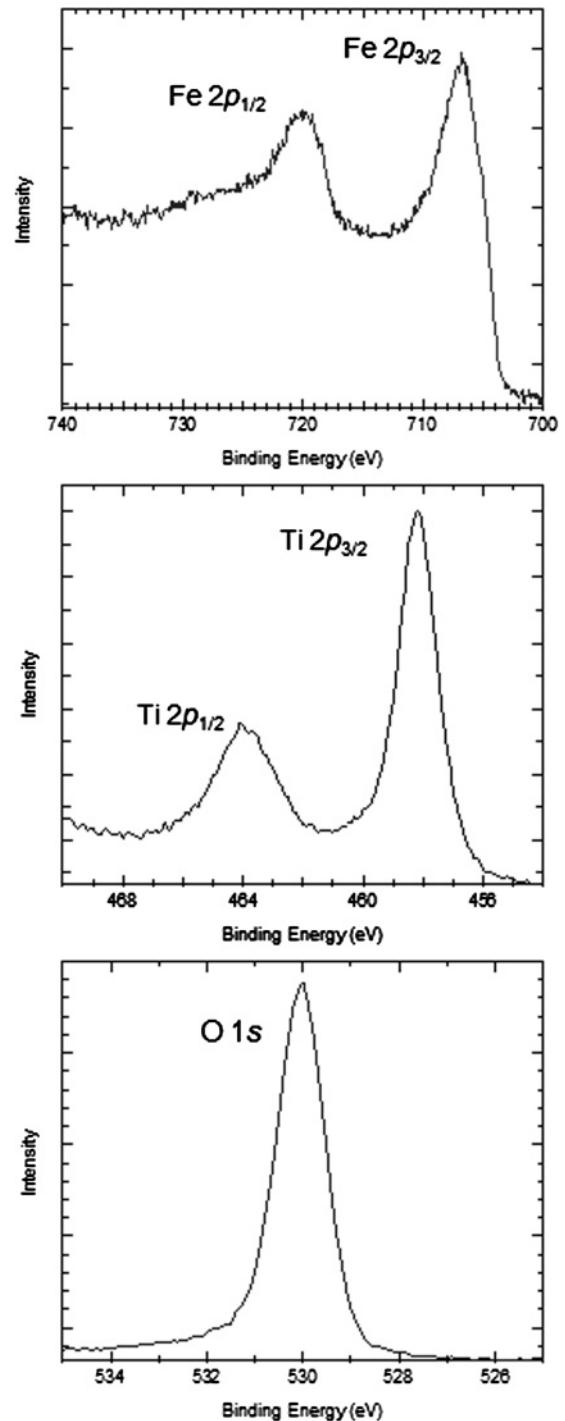


FIG. 5. Al-*K* α -excited XPS spectra obtained for a plasma-cleaned Fe₂TiO₄/MgO(001) film from (top) the Fe 2*p* core-level, (middle) the Ti 2*p* core level, and (bottom) the O 1*s* core level.

before and after heating, either under high-vacuum in an XPS chamber or in an anoxic N₂ atmosphere glove-box (<1 ppm O₂).

For initial XPS analysis, the films were plasma cleaned prior to analysis to remove adventitious carbon. A normal-emission geometry was used to maximize the probing depth. Figure 5 shows XPS regional scan spectra obtained on the Fe₂TiO₄ film for the Fe 2*p* [Fig. 5(a)], Ti 2*p* [Fig. 5(b)], and O 1*s*

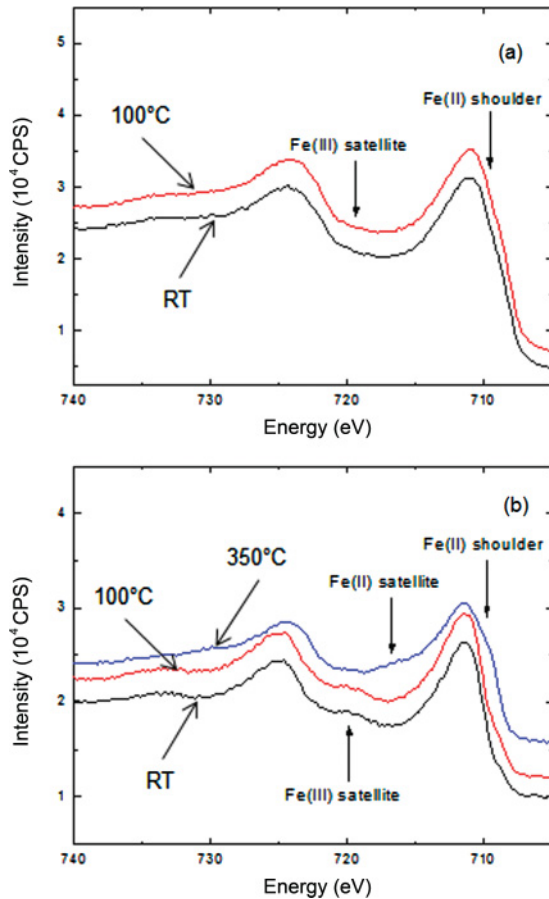


FIG. 6. (Color online) Al- $K\alpha$ -excited XPS spectra obtained for as-synthesized (a) $\text{Fe}_3\text{O}_4/\text{MgO}(001)$ and (b) $\text{Fe}_2\text{TiO}_4/\text{MgO}(001)$ films from the Fe $2p$ core-level region before and after heating to different specified temperatures in the vacuum chamber.

[Fig. 5(c)] core-levels. The Fe $2p$ line shape is complex and inherently broad, but can be used to estimate Fe oxidation states by examination of the satellite structure between the Fe $2p_{3/2}$ and the Fe $2p_{1/2}$ peaks.⁴⁷ The valley between the $2p_{3/2}$ and the $2p_{1/2}$ peaks is filled in or lacking an easily identifiable peak. In addition, there is a slight shoulder on the lower binding energy side of the Fe $2p_{3/2}$ core level. With these two observations the oxidation state of the Fe near the surface is clearly a mixture of Fe(II) and Fe(III),²⁴ consistent with partial-surface oxidation of the Fe_2TiO_4 film. This is not surprising considering the sample was exposed to air during transfer into the XPS analysis chamber and plasma cleaned to remove carbon prior to analysis, allowing for surface oxidation and hydroxylation.^{39,48} The O $1s$ core level is likewise consistent with exposure to water vapor due to the presence of a shoulder roughly 1.5 eV to higher binding energy. The Ti $2p$ core-level line shape shown in Fig. 5(b) indicates that the Ti oxidation state is exclusively Ti(IV). Assuming that the inelastic mean free path of electrons photo ejected from Fe_2TiO_4 by Al- $K\alpha$ x-rays is essentially identical to that for Fe_3O_4 , we expect from prior precedent on XPS of magnetite surface oxidation that the XPS sampling depth is deeper than the surface oxidation/passivation layer.³⁹ Therefore, we can conclude that the entirety of the Ti was in the 4+ oxidation state prior to exposure of the film to air.

Figure 6 shows XPS of as-synthesized Fe_3O_4 [Fig. 6(a)] and Fe_2TiO_4 [Fig. 6(b)] films before and after heating for 10 min under high vacuum ($\sim 5 \times 10^{-9}$ Torr) with an H_2 background gas (4.6×10^{-9} Torr). Here, XPS was performed without plasma cleaning to eliminate any oxidizing effects that could be caused by the oxygen plasma. Also, to enhance surface sensitivity, the photoelectron detector was positioned at 45° off normal. Heating the Fe_3O_4 film to 100°C results in a subtle but detectable increase in the Fe(II) shoulder intensity, indicating reduction of the initial, slightly oxidized surface [Fig. 6(a)]. Estimates of the surface Fe(II) concentration before and after heating are 30% Fe(II) before and 35% Fe(II) after, which indicates reduction to a marginally hyperstoichiometric magnetite surface. In contrast, XPS before and after heating the Fe_2TiO_4 film shows that the surface cannot be fully reduced by heating [Fig. 6(b)]. XPS of the Fe_2TiO_4 film before heating shows an obvious Fe(III) satellite at ~ 720 eV and an Fe(II) shoulder on the lower binding energy side of the Fe $2p_{3/2}$ core level that is less intense relative to the Fe(III) component compared to that of the Fe_3O_4 film [Fig. 6(a)]. Heating the Fe_2TiO_4 film to 100°C results in an increase in the Fe(II) shoulder and the development of an Fe(II) satellite along with a decrease in the Fe(III) satellite. A substantial Fe(III) component consistent with incomplete reduction remains. Even after heating to the PLD growth temperature (350°C), an Fe(III) component is still detectable in the resulting XPS spectrum, demonstrating that it is not possible to reconstitute a completely stoichiometric Fe_2TiO_4 film surface consisting solely of Fe(II) with this approach without Mg out-diffusion from the MgO substrate, which occurs at temperatures greater than 350°C .

The Fe $L_{2,3}$ -edge XAS/XMCD, having a sampling depth of ~ 50 Å, was performed for comparable analysis of the Fe_3O_4 and Fe_2TiO_4 film surface composition. Prior to analysis, the films were heated in an anoxic N_2 atmosphere glove-box (<1 ppm O_2) which, because of an intrinsically higher background O_2 partial pressure in this atmosphere relative to the high vacuum in the XPS chamber, was expected to require a higher heating temperature (300°C for 10 min, as opposed to 100°C) to achieve equivalent levels of surface reduction. Figure 7 shows normalized XAS and XMCD spectra for Fe_3O_4 [Fig. 7(a)] and Fe_2TiO_4 [Fig. 7(b)] films. The XAS and XMCD spectra for the Fe_3O_4 film have characteristics consistent with previous measurements on magnetite,⁴⁹ which for the XMCD spectrum include distinct peaks at ~ 708 (negative), 709 (positive), and 710 (negative) eV assigned to Fe d^6 Oh d^5 Td, and d^5 Oh, respectively. When fit with theoretical component spectra, site occupancy values are estimated as Fe d^6 Oh (1.09):Fe d^5 Td (0.94):Fe d^5 Oh (0.97), very close to the 1:1:1 relative proportions expected for stoichiometric magnetite. This finding is consistent with the XPS analysis of the as-synthesized Fe_3O_4 film, indicating a slightly hyperstoichiometric magnetite surface after heating. For the Fe_2TiO_4 film [Fig. 7(b)], in the XAS spectrum, a substantial increase in the lower energy Fe(II) peak is observed, consistent with Fe(III) reduction to Fe(II) concomitant with Ti(IV) substitution into the cationic sublattice. The intensity reduction of the XMCD signal for this film, measured at 140 K to account for the lower Curie temperature of Ti-rich titanomagnetites,^{50,51} is in agreement with the formation of

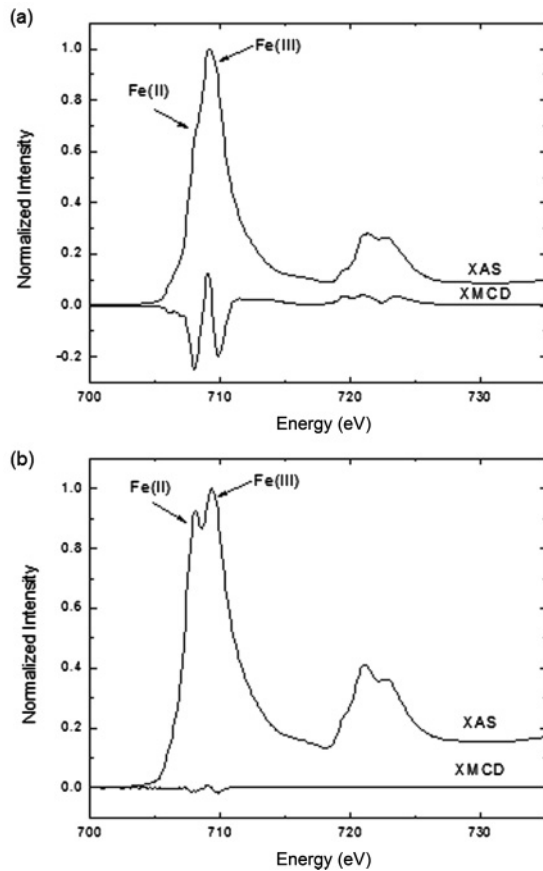


FIG. 7. Fe $L_{2,3}$ XAS absorption spectra of an as-synthesized (a) $\text{Fe}_3\text{O}_4/\text{MgO}(001)$ film and (b) $\text{Fe}_2\text{TiO}_4/\text{MgO}(001)$ film. The averaged L -edge spectra were collected in a reversible 0.6 Tesla magnetic field at 140 K, and the resulting XMCD difference spectra are shown in red.

predominantly end-member ulvöspinel, in which the magnetic structure is antiferromagnetic {zero net magnetization $[\text{Fe}(\text{II})\downarrow]_{\text{A}}[\text{Fe}(\text{II})\uparrow]_{\text{B}}\text{TiO}_4$ }, with minor magnetization consistent with a titanomaghemite-like surface that persists beyond heat treatment in N_2 , yielding the small but measurable XMCD signal.

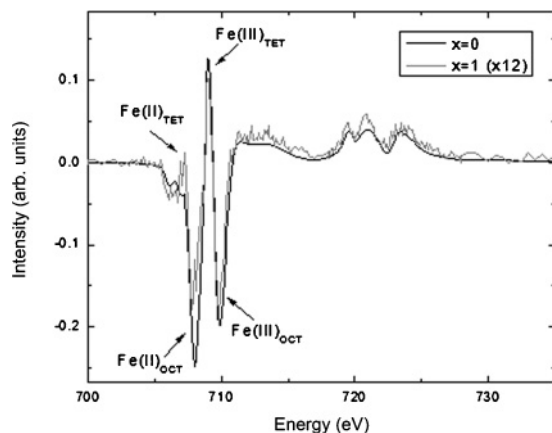


FIG. 8. Fe $L_{2,3}$ -edge XMCD spectra for (black curve) a $\text{Fe}_3\text{O}_4/\text{MgO}(001)$ film and (red curve) a $\text{Fe}_2\text{TiO}_4/\text{MgO}(001)$ film (intensity increased by a factor of 12 for comparison).

As illustrated in more detail in Fig. 8, XMCD of both the Fe_3O_4 and Fe_2TiO_4 films is consistent with expectations for Fe(III) to be replaced by Ti(IV) in the octahedral sublattice and by Fe(II) in the tetrahedral sublattice, producing a peak at ~ 707 eV in the Fe_2TiO_4 spectrum, corresponding to tetrahedral Fe(II).³¹ The surface Fe/Ti ratio, calculated from the edge step of the background-subtracted Fe and Ti $L_{2,3}$ -edge XAS taken consecutively at the same position on the sample, was determined to be ~ 1.13 , which is almost identical to the value of 1.12 calculated from the atomic concentrations given by XPS after heating to 350 °C. This is lower than the expected value of two for Fe_2TiO_4 , suggesting depletion of iron relative to titanium at the surface consistent with indications discussed above that the near surface of the Ti-bearing films tend to possess titanomaghemite-like characteristics. However, alternative contributions cannot yet be ruled out. For example, it is also possible that the low Fe/Ti ratio arises in part from a gradient within the film of Fe and Ti contents in the near surface with an amorphous titanium dioxide surface as the extreme case⁵² but in such low concentrations that it was not detected by Ti K -edge XANES.

IV. CONCLUSION

Epitaxial films of $\text{Fe}_{3-x}\text{Ti}_x\text{O}_4$ from magnetite ($x = 0.0$) to ulvöspinel ($x = 1.0$) were successfully grown on $\text{MgO}(001)$ substrates by off-axis PLD. The bulk of the epitaxial films were of high structural quality and possessed Fe/Ti ratios and a distribution of cationic oxidation states that were close to the desired composition, as shown by RBS and HRXRD. The films were free of secondary phases and large-domain spinodal decomposition. Ti(IV) was found to substitute predominantly for B-site Fe(III), consistent with expectations for this binary series. However, surface-sensitive spectroscopic evidence suggests that the upper few nanometers of the Ti-bearing films were somewhat different to the underlying bulk in terms of Fe/Ti ratio. Surface-sensitive techniques, such as XPS and XMCD, were used to characterize this surface phase and the changes that occurred as a result of (i) oxidation upon air exposure and (ii) reduction upon heating under vacuum or N_2 atmosphere. This paper provides a foundation for production of crystallographically oriented $\text{Fe}_{3-x}\text{Ti}_x\text{O}_4$ films that can be studied for prospective device applications or used to investigate surface reactivity and passivation of these technologically and environmentally significant materials.

ACKNOWLEDGMENTS

This paper was supported by the US Department of Energy Office of Biological and Environmental Research (OBER) as part of OBER's Subsurface Biogeochemistry Research Program (SBR). This contribution originates from the SBR Scientific Focus Area at the Pacific Northwest National Laboratory (PNNL). Some of the research was performed in the Environmental Molecular Sciences Laboratory, a national scientific user facility sponsored by the OBER and located at PNNL. Use of the Advanced Photon Source was supported by the US Department of Energy Office of Science Office of Basic Energy Sciences under Contract No. DE-AC02-06CH11357.

Use of the Advanced Light Source was supported by the Director, Office of Science Office of Basic Energy Sciences, of

the US Department of Energy under Contract No. DE-AC02-05CH11231.

*Corresponding author: kevin.rosso@pnl.gov

¹J. D. Adam, L. E. Davis, G. F. Dionne, E. F. Schloemann, and S. N. Stitzer, *IEEE Trans. Microwave Theory Tech.* **50**, 721 (2002).

²S. Picozzi and C. Ederer, *J. Phys.: Condens. Matter* **21**, 303201 (2009).

³Y. Suzuki, *Annu. Rev. Mater. Res.* **31**, 265 (2001).

⁴F. Bosi, U. Halenius, and H. Skogby, *Am. Mineral.* **93**, 1312 (2008).

⁵Z. Hauptman and A. Stephens, *J. Phys. E* **1**, 1236 (1968).

⁶F. Bosi, U. Halenius, and H. Skogby, *Am. Mineral.* **94**, 181 (2009).

⁷V. A. M. Brabers, *Physica B* **205**, 143 (1995).

⁸A. A. Cristobal, E. F. Aglietti, M. S. Conconi, and J. M. P. Lopez, *Mater. Chem. Phys.* **111**, 341 (2008).

⁹A. A. Cristobal, E. F. Aglietti, J. M. P. Lopez, F. R. Sives, and R. C. Mercader, *J. Eur. Ceram. Soc.* **28**, 2725 (2008).

¹⁰M. J. Rossiter and P. T. Clarke, *Nature* **207**, 402 (1965).

¹¹A. B. Woodland and B. J. Wood, *European Journal of Mineralogy* **6**, 23 (1994).

¹²A. Bollero, M. Ziese, R. Hohne, H. C. Semmelhack, U. Kohler, A. Setser, and P. Esquinazi, *J. Magn. Magn. Mater.* **285**, 279 (2005).

¹³M. Sorescu, A. Grabias, D. Tarabasanu-Mihaila, and L. Diamandescu, *Appl. Surf. Sci.* **217**, 233 (2003).

¹⁴G. D. Price, *Am. Miner.* **66**, 751 (1981).

¹⁵S. A. Chambers, *Surf. Sci. Rep.* **39**, 105 (2000).

¹⁶T. Kado, *Thin Solid Films* **459**, 187 (2004).

¹⁷A. Nielsen, A. Brandlmaier, M. Althammer, W. Kaiser, M. Opel, J. Simon, W. Mader, S. T. B. Goennenwein, and R. Gross, *Appl. Phys. Lett.* **93**, 162510 (2008).

¹⁸M. L. Parames, J. Mariano, Z. Viskadourakis, N. Popovici, M. S. Rogalski, J. Giapintzakis, and O. Conde, *Appl. Surf. Sci.* **252**, 4610 (2006).

¹⁹S. Tiwari, R. J. Choudhary, and D. M. Phase, *Thin Solid Films* **517**, 3253 (2009).

²⁰H. Murase, K. Fujita, S. Murai, and H. Tanaka, *J. Physics: Conf. Series* **200**, 062013 (2009).

²¹H. Murase, K. Fujita, S. Murai, and K. Tanaka, *Mater. Trans.* **50**, 1076 (2009).

²²S. S. Perry, H. I. Kim, S. Imaduddin, S. M. Lee, and P. B. Merrill, *J. Vac. Sci. Technol. A* **16**, 3402 (1998).

²³S. S. Perry and P. B. Merrill, *Surface Science* **383**, 268 (1997).

²⁴Y. Gao, Y. J. Kim, and S. A. Chambers, *J. Mater. Res.* **13**, 2003 (1998).

²⁵Y. J. Kim, Y. Gao, and S. A. Chambers, *Surface Science* **371**, 358 (1997).

²⁶M. Mayer, *AIP Conf. Proc.* **475**, 541 (1999).

²⁷E. S. Ilton, J. F. Boily, E. C. Buck, F. N. Skomurski, K. M. Rosso, C. L. Cahill, J. R. Bargar, and A. R. Felmy, *Environ. Sci. Technol.* **44**, 170 (2010).

²⁸E. Arenholz and S. O. Prestemon, *Rev. Sci. Instrum.* **76**, 083908 (2005).

²⁹S. Gota, M. Gautier-Soyer, and M. Sacchi, *Phys. Rev. B* **62**, 4187 (2000).

³⁰R. A. D. Patrick, G. Van der Laan, C. M. B. Henderson, P. Kuiper, E. Dudzik, and D. J. Vaughan, *Eur. J. Mineral.* **14**, 1095 (2002).

³¹C. I. Pearce, C. M. B. Henderson, N. D. Telling, R. A. D. Patrick, J. M. Charnock, V. S. Coker, E. Arenholz, F. Tuna, and G. van der Laan, *Am. Mineral.* **95**, 425 (2010).

³²G. Vanderlaan and I. W. Kirkman, *J. Phys. Condens. Matter* **4**, 4189 (1992).

³³G. Vanderlaan and B. T. Thole, *Phys. Rev. B* **43**, 13401 (1991).

³⁴R. F. C. Farrow, P. M. Rice, M. F. Toney, R. F. Marks, J. A. Hedstrom, R. Stephenson, M. J. Carey, and A. J. Kellock, *J. Appl. Phys.* **93**, 5626 (2003).

³⁵M. L. Parames, Z. Viskadourakis, M. S. Rogalski, J. Mariano, N. Popovici, J. Giapintzakis, and O. Conde, *Appl. Surf. Sci.* **253**, 8201 (2007).

³⁶S. A. Chambers, S. Thevuthasan, and S. A. Joyce, *Surface Science* **450**, L273 (2000).

³⁷B. Stanka, W. Hebenstreit, U. Diebold, and S. A. Chambers, *Surface Science* **448**, 49 (2000).

³⁸R. Pentcheva, F. Wendler, H. L. Meyerheim, W. Moritz, N. Jedrecy, and M. Scheffler, *Phys. Rev. Lett.* **94**, 126101 (2005).

³⁹T. Kendelewicz, P. Liu, C. S. Doyle, G. E. Brown, E. J. Nelson, and S. A. Chambers, *Surface Science* **453**, 32 (2000).

⁴⁰F. de Groot, G. Vanko, and P. Glatzel, *J. Phys. Condens. Matter* **21**, 104207 (2009).

⁴¹S. DeBeer George, P. Brant, and E. I. Solomon, *J. Am. Chem. Soc.* **127**, 667 (2004).

⁴²J. M. Thomas and G. Sankar, *Acc. Chem. Res.* **34**, 571 (2001).

⁴³D. Morris, Y. Dou, J. Rebane, C. E. J. Mitchell, R. G. Egdell, D. S. L. Law, A. Vittadini, and M. Casarin, *Phys. Rev. B* **61**, 13445 (2000).

⁴⁴S. Aggarwal and R. Dieckmann, *Phys. Chem. Miner.* **29**, 695 (2002).

⁴⁵W. O'Reilly, *Phys. Earth Planet. Inter.* **31**, 65 (1983).

⁴⁶W. X. Xu, D. R. Peacor, W. A. Dollase, R. VanDerVoo, and R. Beaubouef, *Am. Mineral.* **82**, 1101 (1997).

⁴⁷T. Droubay and S. A. Chambers, *Phys. Rev. B* **64**, 205414 (2001).

⁴⁸S. A. Krasnikov, A. S. Vinogradov, K. H. Hallmeier, R. Hohne, M. Ziese, P. Esquinazi, T. Chasse, and R. Szargan, *Mater. Sci. Eng. B* **109**, 207 (2004).

⁴⁹C. I. Pearce, C. M. B. Henderson, R. A. D. Patrick, G. Van der Laan, and D. J. Vaughan, *Am. Miner.* **91**, 880 (2006).

⁵⁰S. Akimoto, *J. Phys. Soc. Jpn.* **17**, 706 (1962).

⁵¹Z. Kakol, J. Sabol, and J. M. Honig, *Phys. Rev. B* **43**, 649 (1991).

⁵²P. Perriat, E. Fries, N. Millot, and B. Domenichini, *Solid State Ionics* **117**, 175 (1999).